Comprehensive vibrational spectroscopic characterization of nylon-6 precursors for precise tracking of the Beckmann rearrangement

Stephanie Chapman, Alexander J. O'Malley,
Stewart F. Parker and Robert Raja

Published version information

This is the peer reviewed version of the following article:

S Chapman et al. "Comprehensive vibrational spectroscopic characterization of nylon-6 precursors for precise tracking of the Beckmann rearrangement." ChemPhysChem, vol.19, no. 23 (2018): 3196-3203.

DOI: 10.1002/cphc.201800721

Which has been published in final form at DOI above. This article may be used for non-commercial purposes in accordance with Wiley-VCH terms and conditions for self-archiving.

Please cite only the published version using the reference above. This is the citation assigned by the publisher at the time of issuing the AAM. Please check the publisher's website for any updates.

Comprehensive vibrational spectroscopic characterization of nylon-6 precursors for precise tracking of the Beckmann rearrangement

Stephanie Chapman,[a] Alexander J. O'Malley,[b,c,d] Stewart F. Parker,[d,e] and Robert Raja *[a,d]

Abstract: As a key step in nylon-6 synthesis, the Beckmann rearrangement is an ongoing target of catalytic studies that seek to improve the sustainability of polymer manufacture. Whilst solid-acid catalysts (predominantly zeotypes) have proven effective for this transformation, the development of more active and selective systems demands an understanding of fundamental catalytic mechanisms. In this undertaking, *in situ* and *operando* characterization techniques can be informative, provided rigorous spectroscopic groundwork is in place. Thus, to facilitate mechanistic studies we present a detailed investigation of the vibrational spectra of cyclohexanone oxime, ε-caprolactam and their D10-isotopomers, in the solid state. Variable-temperature infrared (150 – 300 K) and Raman (10 – 300 K) spectra are reported alongside inelastic neutron scattering data. Moreover, where key vibrational modes have been assigned with the aid of periodic density functional theory calculations, it has been possible to include hydrogen-bonding interactions explicitly.

Introduction

As the first synthetic polymers to be manufactured commercially, the polyamides, or nylons, remain some of the most industrially and economically significant synthetic fibers in large-scale production.[1] Nylon-6, in particular, has found extensive use in engineering plastics and fibers - applications that exploit its characteristic ductility, strength, and resistance to physical and chemical degradation. Accordingly, global demand for nylon-6 is expected to reach 7690 megatonnes by 2026.[2]

[a] S. Chapman, Prof R. Raja
School of Chemistry, University of Southampton
University Road, Southampton, SO17 1BJ, UK.
R.Raja@soton.ac.uk
[b] Dr A. J. O'Malley
Centre for Sustainable Chemical Technologies (CSCT),
Department of Chemistry,University of Bath,
Bath, BA2 7AY, UK.
[c] Dr A. J. O'Malley
Cardiff Catalysis Institute, School of Chemistry, Cardiff University,
Main Building, Park Place, Cardiff, CF10 3AT, UK.
[d] Prof R. Raja, Dr A. J. O'Malley, Dr S. F. Parker
UK Catalysis Hub, Research Complex at Harwell, Science and
Technology Facilities Council Rutherford Appleton Laboratory,
Harwell Science and Innovation Campus, Oxon OX11 0QX, UK.
[e] Dr S. F. Parker
ISIS Pulsed Neutron and Muon Facility
Science and Technology Facilities Council Rutherford Appleton
Laboratory, Harwell Science and Innovation Campus, Oxon OX11
0QX, UK.

Supporting information for this article is given via a link at the end of the document.

Nylon-6 is produced by the ring-opening polymerization of the cyclic amide, ε-caprolactam (Figure 1). As the key intermediate in the production of nylon-6, ε-caprolactam is a high-value bulk chemical and its global production was predicted to exceed 4.6 million tonnes in 2017.[3] Typically, ε-caprolactam is produced by the acid-catalyzed Beckmann rearrangement of cyclohexanone oxime (itself generated from cyclohexanone). The conventional, industrial Beckmann rearrangement is effected by a harsh mineral acid catalyst in a multi-step process that generates stoichiometric quantities of ammonium sulfate by-product.[4] As this is both hazardous and inherently uneconomical, traditional homogenous acid catalysts are being superseded by heterogeneous alternatives.[5] As well as offering ease of recoverability from the fluid-phase reaction, solid-acid catalysts eliminate the need for aggressive reagents, simultaneously mitigating the vast quantities of low-value by-product associated with the conventional process.[6] Zeolite and zeotype catalysts have had particular success in this domain,[5] offering a robust, porous framework with tunable acid characteristics. By invoking weak acid sites, such as the silanol nests in zeolite H-ZSM-5,[7] or Brønsted acid centers in silicoaluminophosphates (SAPOs),[8] it has been possible achieve high yields in the Beckmann rearrangement.

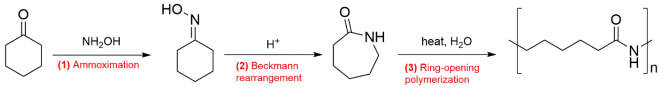

Figure 1. Scheme depicting the synthesis of nylon-6. The ammoximation of cyclohexanone yields cyclohexanone oxime (1), which undergoes an acid-catalyzed Beckmann rearrangement to form ε-caprolactam (2). Subsequent ring-opening polymerization of ε-caprolactam (3) yields nylon-6.

When optimizing catalysts for chemical transformations such as the Beckmann rearrangement, an understanding of catalyst mechanism is advantageous. Whilst advances in characterization (especially *in situ* and *operando*) techniques continue to provide detailed insight into catalyst operation, the process of extracting useful information can be hindered by the need for fundamental, but often demanding analyses to be in place. Illustratively, the vibrational characterization of cyclohexanone oxime and ε-caprolactam (unlike cyclohexanone)[9] is notably lacking, despite their importance as intermediates in nylon-6 manufacture. Namely, infrared spectroscopy has been used monitor the heterogeneously-catalyzed Beckmann transformation (e.g.[10]), and the infrared and Raman spectra of cyclohexanone oxime and ε caprolactam (supported by density functional theory (DFT) calculations) have been reported as part of the measurement of thermodynamic properties (heats of sublimation and vaporization, and the standard entropy) in the ideal gas state.[11] Infrared spectroscopy has also been used to study hydrogen bonding in cyclohexanone oxime, both in solution and in the solid state.[12]

Nonetheless, vibrational spectra have been assigned using normal coordinate analysis[13] and DFT,[14] invoking the isolated molecule approximation so that hydrogen bonding is omitted or only treated empirically - even when the experimental data is for the solid state. Whilst studies into the effect of hydrogen bonding and conformation on the resonance Raman spectrum of ε-caprolactam are extensive, such investigations have been confined to the solution phase.[14-15]

Therefore, to support future studies into the mechanism of Beckmann rearrangement process, we present a comprehensive investigation of the vibrational spectra of cyclohexanone oxime, ε-caprolactam and their D10-isotopomers (giving increased clarity to the relevant functional groups) in the solid state. Variable-temperature infrared (150 – 300 K) and Raman (10 – 300 K) spectra are recorded together with inelastic neutron scattering (INS) spectra. Assignments are made with the aid of periodic density functional theory (DFT) calculations of the solid-state structures and thus hydrogen-bonding is explicitly included.

Results and Discussion

In the following sub-sections, we briefly review the spectroscopy of cyclohexanone, before presenting a complete assignment of both cyclohexanone oxime and its ring-deuterated, D10-isotopomer, and ε-caprolactam and its D10-isotopomer. Finally, we compare the spectra of cyclohexanone, cyclohexanone oxime, and ε-caprolactam to highlight the characteristic and distinctive modes of each species.

Cyclohexanone

Below the melting point of 245 K, cyclohexanone forms a face-centered, cubic, plastic crystal of the space group $Fm\bar{3}m$. However, on cooling to below 225 K, the crystal transforms to the ordered, monoclinic, Phase III structure of the space group $P2_1/n$.[16] (The orthorhombic Phase II exists under high pressure, but the triple point for all three phases is close to ambient pressure). The vibrational spectra of the liquid phase have been comprehensively studied and assigned by both normal coordinate[9a] and isolated molecule DFT[9c] calculations, and solid-state transitions have been investigated by infrared and Raman spectroscopies.[9b]

The INS spectrum of cyclohexanone - hitherto unreported in the literature - is presented in Figure 2a alongside periodic-DFT calculation of Phase III for the Γ-point only (Figure 2b), and for the entire Brillouin zone (Figure 2c). Above 300 cm^{-1}, the agreement between experimental and calculated spectra is essentially quantitative. However, at ~ 200 cm^{-1} a mode that is clearly split in the experimental spectrum is calculated as a single peak. The dispersion (i.e. the variation of transition energy with wavevector) curves for the low energy region (Figure 3, with the full range shown in Figure S4) reveal little dispersion; rather the discrepancy arises from underestimating the calculated factor group splitting (5 cm^{-1}) versus that observed (15 cm^{-1}).

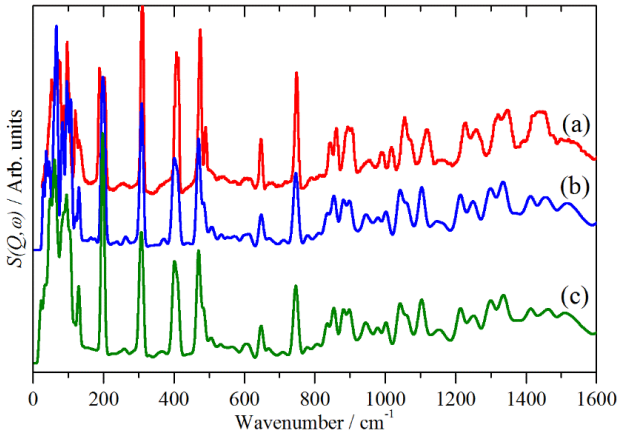

Figure 2. INS spectra of (a) cyclohexanone in Phase III at 10 K and as calculated using CASTEP: (b) Γ-point only and (c) for the entire Brillouin zone.

The low energy region below 200 cm^{-1} is complex and poorly represented by the Γ-point-only calculation, but shows better agreement with the entire-Brillouin-zone calculation. Discrepancies in the low-energy region are attributed to a modest dispersion (< 20 cm^{-1}) in all modes, which arises due to (albeit relatively weak) intermolecular interactions: cyclohexanone possesses a significant dipole moment of 2.87 D,[17] such that in $C_6D_{10}O$[16] there are four O•••D connections in the range 2.48–2.59 Å.

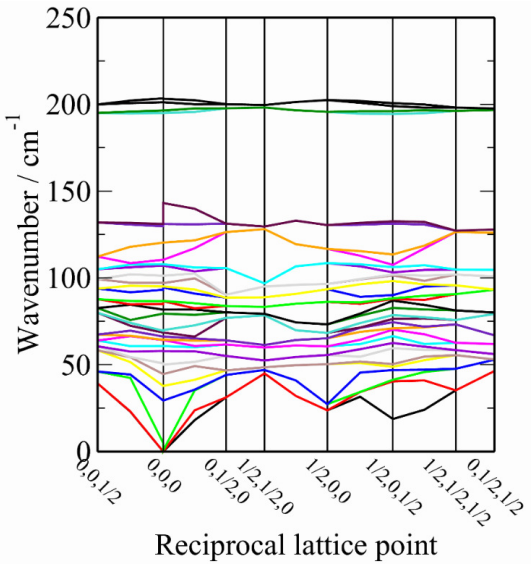

Figure 3. Calculated dispersion curves of cyclohexanone in Phase III.

In the gas phase, cyclohexanone has C_s symmetry.[18] In the solid state this is largely retained,[16] and modes involving atoms that lie outside of the mirror-plane form symmetric and (in-phase) and asymmetric (out-of-phase) pairs. A complete assignment of modes in the 0 – 1800 cm^{-1} region (Table S2) reveals a divide between the external modes (translations and librations) and the

internal modes at ~120 cm^{-1}. The key modes associated with the carbonyl functionality occur at ~1700 cm^{-1} (C=O stretch), 490 cm^{-1} (C=O in-plane bend) and 130 cm^{-1} (C=O out-of-plane bend). Although the C=O stretch is not observed in the INS spectrum because it largely involves motion of atoms with modest cross sections, it is readily apparent in both the infrared and Raman spectra. As noted previously,[9a] there is extensive mixing of modes, particularly of the C–C stretch modes with the methylene rock, wag and twist modes. Our assignment of the vibrational spectrum of cyclohexanone in the solid state both confirms and extends previous work[9a, 9b] that uses the isolated molecule approximation.

Cyclohexanone oxime

Much like cyclohexanone,[16] solid-state cyclohexanone oxime exhibits structural polymorphism. However, unlike its synthetic precursor, cyclohexanone oxime has not been subject to detailed structural characterization. Heat capacity measurements[11b] reveal two reversible solid-solid transitions at 241.5 and 301.5 K, and a melting point of 362.0 K. For cyclohexanone-D10 oxime (Figure S5), these transitions occur at a marginally higher temperature (242.3, 302.5 and 364.4 K). Thus, from these measurements, three crystalline phases can be defined: Phase III < 241.5 K < Phase II < 301.5 K < Phase I < 364.4 K.

The only investigation[19] of the room temperature Phase I, found a hexagonal structure, $P6_3$ (no. 173), with six formula units in the unit cell, comprising of two trimers of cyclohexanone oxime. The lowest energy conformation of cyclohexanone oxime (Figure 4A) has two forms: the chair (C) and the inverted chair (I). This, in turn, gives rise to four possible trimers: CCC, CCI (shown in Figure 4B), CII and III, with significant disorder along the *c*-axis being ascribed to a random distribution of these trimers.

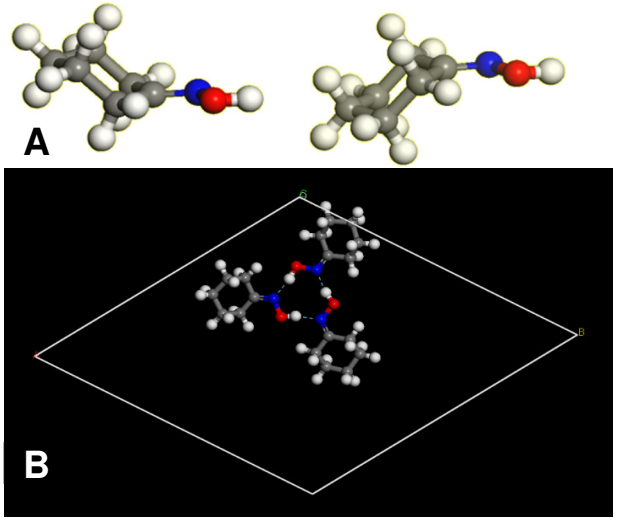

Figure 4. A) Left: the chair (C) and right: the inverted (I) chair conformation of cyclohexanone oxime, and **B**) the trimer motif that is characteristic of all three phases of cyclohexanone oxime (hydrogen bonds shown as dashed lines), viewed along the *c*-axis of the fully ordered, low-temperature Phase III (CCI), with five of the trimers removed.

We are unaware of any structural investigation of Phase II, but the structure of cyclohexanone oxime in Phase III has been determined several times despite complications due to twinning. The most recent determination at 110 K successfully resolved this problem, revealing a centrosymmetric structure in the trigonal space group $P\bar{3}$ (no. 147), with 18 formula units per primitive cell.[20] Closer inspection of this Phase III structure reveals two layers of six trimeric oxime units, in the CCI arrangement.

Vibrational studies of cyclohexanone oxime clearly demonstrate the aforementioned phase changes. These are most apparent in the Raman spectra of the all-H species (Figure 5), and the infrared spectra of the D10 species (Figure 6). (The infrared spectra of the all-H and the Raman spectra of the D10 are reported in Figures S6 and S7, respectively). In the Raman spectra (Figure 5), a progressive sharpening of the bands in the sequence: Phase I → Phase II → Phase III is most obvious for the lattice modes, 0 – 200 cm^{-1}, and the bands around 1400 cm^{-1}. Similarly, in the infrared spectra (Figure 6), the relative intensities of the O–H stretch modes at 2700 – 3600 cm^{-1} progressively sharpen. The changes on transforming from Phase I to Phase II are subtle but reproducible, and the similarity of the Phase II structure to the other phases of cyclohexanone oxime indicate that the trimer motif is maintained.

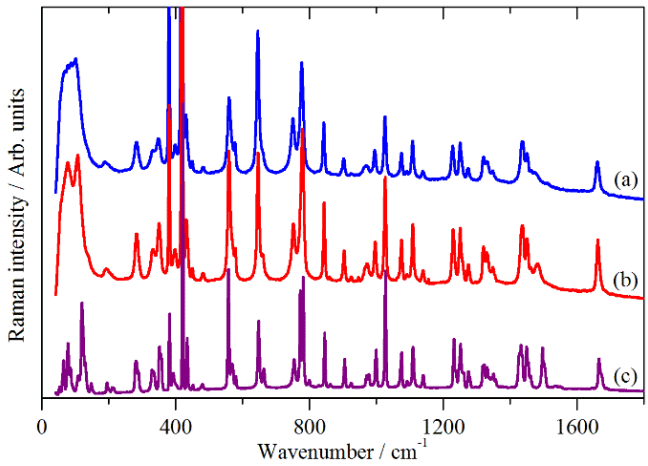

Figure 5. The Raman spectra of cyclohexanone oxime in (a) Phase I, 320 K, (b) Phase II, 270 K and (c) Phase III, 10 K.

Structural changes in solid cyclohexanone oxime show increasing order with decreasing temperature. Therefore, whilst Phase I is a mixture of all four possible trimers, Phase III consists exclusively of one form. Phase II then, presumably represents the intermediate case where there is still more than one form of trimer. Calculation of the energies of the trimers using the model shown in Figure 4, finds that they are almost degenerate: III 0, CCC +1.22 meV (+1.95 x10^{-22} J), CII +4.74 meV (+7.59 x10^{-22} J), CCI +10.11 meV (+1.62 x10^{-21} J), (energies relative to the lowest energy trimer). Somewhat surprisingly, it is not the lowest energy trimer that occurs in Phase III, but the highest energy one. The implication is that whilst the interaction between the trimers is weak, it is still sufficient to offset the energy difference. Therefore,

band sharpening is attributed, in part, to the decreasing temperature, but also to increasing order in the structure. This is particularly apparent in the lattice modes, which are akin to those of an amorphous system in Phase I, and yet resemble a crystalline material in Phase III.

Figure 6. The infrared spectra of cyclohexanone-D10 oxime in (a) Phase I, 323 K, (b) Phase II, 286 K and (c) Phase III, 140 K.

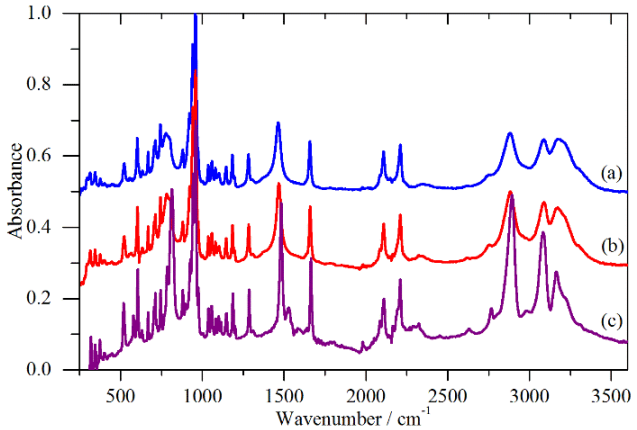

In the context of the Beckmann rearrangement process, the oxime functionality (C=N–O–H) is of particular interest. The characteristic modes are the O–H, C=N and N–O stretch modes, and the in-plane and out-of-plane N–O–H deformation modes. The high-energy region for the Phase III structure of the all-H and D-10 oxime is presented in Figure 7, and includes all three types of vibrational spectroscopy.

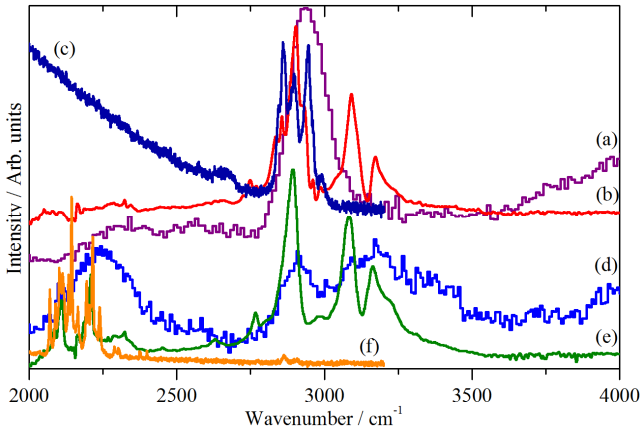

Figure 7. Vibrational spectra of Phase III at 10 K in the C–D/-/O–H stretch region of cyclohexanone oxime: (a) INS, (b) infrared, (c) Raman, and cyclohexanone-D10 oxime: (d) INS, (e) infrared and (f) Raman. Note that (d) is ×10 ordinate expanded relative to (a).

For the all-H species, the Raman and INS spectra in this region are dominated by C–H stretch modes. Where the infrared spectrum of cyclohexanone-H10 oxime shows two modes at 3091 and 3174 cm^{-1}, comparison with the D-10 analogue reveals that these modes, and another at 2895 cm^{-1}, are obscured by C–H stretches. The three O–H stretch modes of the trimer would give rise to a totally symmetric (*A*) and a doubly degenerate (*E*) mode if a C_3 symmetry axis were present, but the CCI configuration of the trimer lifts such degeneracy. We therefore assign the lowest energy mode as the totally-symmetric, in-phase O–H stretch, and the two highest modes as the split *E*-mode. INS spectroscopy supports this assignment, since the area of the high-energy feature is approximately twice that of the 2895 cm^{-1} mode (note that Figure 7d is ×10 ordinate expanded relative to Figure 7a). In the INS spectrum of the all-H species, the combination of the coincidence of the C–H and O–H stretch modes, the tenfold excess of C–H modes, and the width of the O–H stretch modes makes this feature essentially invisible.

The C=N stretch, which typically occurs at around 1660 cm^{-1},[21] is seen in both the infrared and Raman spectra of cyclohexanone oxime (Figures 5, 6, S6 and S7). The N–O stretch, which occurs at approximately 900 cm^{-1},[22] is often the strongest band in the spectrum, as exemplified here. The N–O–H deformation modes are most readily detected by INS (Figure 8), particularly in the D-10 species where they dominate the spectrum by virtue of the tenfold larger cross section of H *versus* D. The in-plane mode N–O–H occurs at 1490 cm^{-1} and the out-of-plane mode at 792 cm^{-1}. Thus, it is through the combination of three types of spectroscopy that a complete assignment of the vibrational characteristics of cyclohexanone oxime can be made.

Figure 8. INS spectra in Phase III at 10 K of (a) cyclohexanone oxime, (b) cyclohexanone oxime as calculated using CASTEP, (c) cyclohexanone-D10 oxime and (d) as calculated using CASTEP. Note that (c) is ×11 ordinate expanded relative to (a), reflecting the difference in cross section between H and D. The CASTEP spectra are for the complete unit cell of 342 atoms.

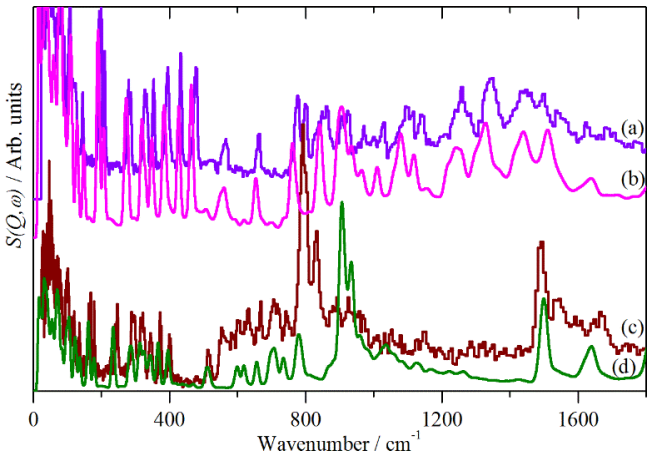

The complex structure of solid-state cyclohexanone oxime makes computational studies challenging. However, the trimer motif that is common to the three solid phases of the oxime is probably also maintained in solution.[19] In Phase III, the closest contact within a layer is at 2.6 Å, and between layers is at 2.4 Å (in both cases through non-linear H···H contacts), indicating that there is little interaction between the oxime trimers. Therefore, to make the DFT calculations tractable, and to be representative of all three

solid phases, five of the six trimers were removed in order to reduce the number of atoms from 342 to 57. The resulting model is shown in Figure 4B. Comparison of experimental and calculated INS spectra is a stringent test of a model,[23] hence Figure S8 compares the observed and calculated spectra for the all-H and the D-10 species. Whilst the correspondence between calculated and experimental spectra is reasonable for INS, for the infrared spectra (Figure S9a, b) the results are unsatisfactory. The indication is that the interactions between the oxime trimers (although weak) are significant and have observable spectroscopic consequences. Further investigation showed that it was possible, albeit time consuming, to use the complete structure containing 342 atoms.[22] Figure 8 shows a comparison of the observed and calculated INS spectra for the all-H and the D-10 species, and the calculated infrared spectrum is shown in Figure S9c. The only significant difference between the observed and calculated spectra in Figure 8 is for the N–H out- of-plane mode at ~ 800 cm^{-1}. This is most apparent for the D10 species, and due to the use of the PBE functional, which results in overbinding of the hydrogen bonds: experimental O–H•••N = 2.763, 2.765 and 2.783 Å, calculated O–H•••N = 2.703, 2.713 and 2.720 Å. This has been observed previously for H_2O_2,[24] $CsHSO_4$,[25] and a series of amines and amine hydrochlorides;[26] nonetheless, this relatively inexpensive GGA functional has allowed us to fully assign the vibrational spectrum.

The presence of 18 molecules in the unit cell results in 18 factor group components for each mode. Inspection of the calculated transition energies shows that for the internal modes, the splitting is generally less than 15 cm^{-1}. Table S3 presents a complete assignment of the spectra of both the all-H and the D-10 species; for each mode the average of the 18 factor group components is given as the calculated transition energy, together with range of transition energies: highest in factor group – lowest in factor group. The only exception is for the O–H stretch modes which splits into three distinct groups of six, alluding to the *A + E* splitting of an idealized C_3 structure.

Unlike cyclohexanone, cyclohexanone oxime does not possess a mirror plane and thus, in principle, each methylene group could behave as an independent entity. However, visualization of the normal modes shows that, in practice, this only occurs for the C–H stretch region. For the deformation modes, the methylene vibrations are similar to those of cyclohexanone, with each methylene group forming in-phase and out-of-phase pairs with its 'mirror' image.

ε-Caprolactam

In contrast to cyclohexanone and cyclohexanone oxime, the solid state behavior of ε caprolactam is relatively straightforward. Differential scanning calorimetry (DSC) studies by ourselves (Figure S5) and others,[27] show no evidence of a phase transition between 5 K and the melting point (342.3 K). A comparison of the Raman spectra recorded at 300 K and 10 K (Figure S8) supports this conclusion since, beyond the expected sharpening of the bands at 10 K, the spectra are identical. Solid ε-caprolactam has a monoclinic structure in the centrosymmetric space group *C2/c*, with four molecules in the primitive cell.[28] These each form centrosymmetric dimers with molecules in neighboring cells.

Figures 9 and 10 show the vibrational spectra of the all-H and the D-10 caprolactam species, respectively. The spectra in the N–H stretch are unexpectedly complex. Four molecules in the primitive cell of a centrosymmetric structure gives rise to two infrared active, and two Raman active N–H stretching modes. However, as highlighted by the infrared spectrum of the D10 species (Figure 10a), there are at least five bands in this region. ε-Caprolactam is an example of a secondary amide with a *cis* configuration of the C=O and N–H bonds. These typically exhibit the N–H stretch at ~3200 cm^{-1} and a combination mode of the C=O and N–H stretches at ~3100 cm^{-1},[21] the intensity of latter being enhanced by Fermi resonance with the N–H stretch. Both features are present in our spectra at 3198 and 3056 cm^{-1}, respectively.

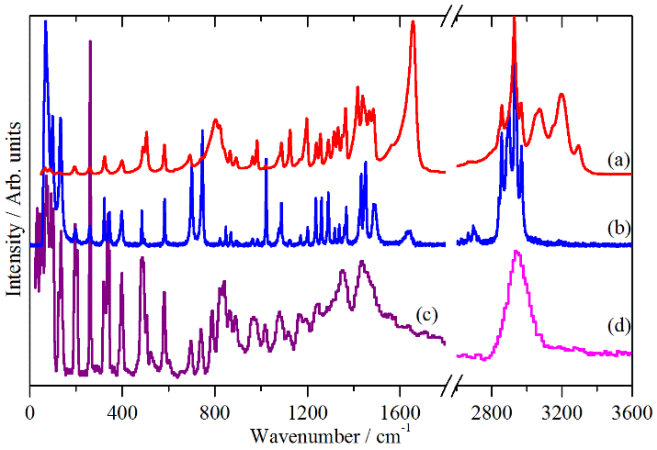

Figure 9. Vibrational spectra of ε-caprolactam: (a) infrared (RT), (b) FT-Raman (RT) and INS (20 K) recorded on (c) TOSCA, 0 – 2500 cm^{-1}, and (d) MAPS, 2500 – 3600 cm^{-1}.

The weaker features at 2895, 2931 and 3280 cm^{-1} are assigned as: 1408 + 1471 cm^{-1}, 2 × 1471 cm^{-1} and 2 × 1646 cm^{-1}, respectively, presumably all in Fermi resonance with the N–H stretch mode. These combinations all involve the characteristic modes of a lactam: 1408 cm^{-1} = C_1–N stretch, 1471 cm^{-1} = N–H in-plane bend and 1646 cm^{-1} = C=O stretch. The out-of-plane bend is obvious in the 300 K infrared spectra (Figures 9a, 10a) as a broad feature at 801 cm^{-1}. In the INS spectrum of the D-10 species at 10 K, it is resolved into two components at 793 and 831 cm^{-1}.

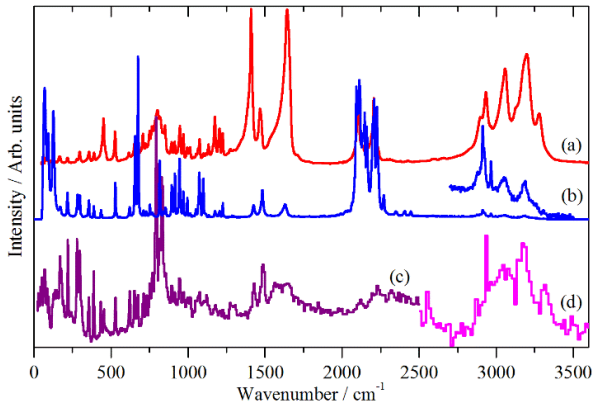

Figure 10. Vibrational spectra of ε-caprolactam-D10: (a) infrared (RT), (b) FT-Raman (RT), the inset is a ×10 ordinate expansion of the 2700 – 3600 cm^{-1} region and INS (20 K) recorded on (c) TOSCA, 0 – 2500 cm^{-1}, and (d) MAPS, 2500 – 3600 cm^{-1}.

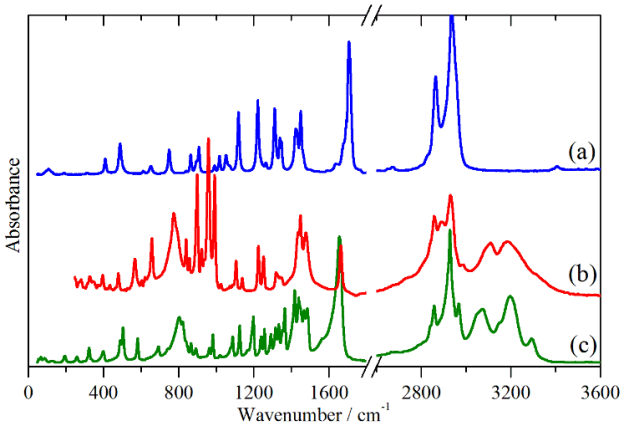

Figure 12. Comparison of room-temperature infrared spectra of: (a) cyclohexanone, (b) cyclohexanone oxime and (c) ε-caprolactam.

Periodic-DFT calculations confirm the aforementioned assignments. Figure 11 shows a comparison of the observed and calculated INS spectra, with assignments reported in Table S4. The C_1 molecular symmetry means that the mode descriptions are over-simplified and the modes are highly mixed. As these calculations do not aid the assignment of C–H or C–D stretch modes, only the N–H related modes are reported in Table S4. As in cyclohexanone oxime, the strength of the hydrogen bonds are overestimated by these calculations: experimental N–H•••O = 2.895 Å *versus* calculated N–H•••O = 2.844 Å.

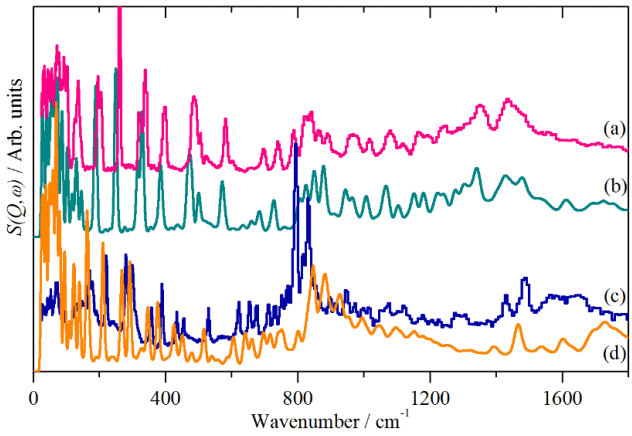

Figure 11. INS spectra at 10 K of ε-caprolactam (a) experimental, (b) as calculated using CASTEP and ε-caprolactam-D10 (c) experimental and (d) as calculated using CASTEP.

Comparison of spectra

The vibrational spectra of cyclohexanone, cyclohexanone oxime and ε-caprolactam are compared in Figures 12-14. Simply by inspecting the patterns of the spectra, it would appear that distinguishing the three compounds is straightforward. This is certainly true for the pure materials, however, our interest[8a] lies in understanding how they interact with the porous, acid catalysts that are increasingly employed for the rearrangement process.[5] In this case, the problem becomes much more complex, since the amount of information is greatly reduced. Thus, infrared spectra are only available for > 1600 cm^{-1} due to absorption of radiation by the catalyst lattice. Even characteristic modes (e.g. the cyclohexanone C=O stretch at 1707 cm^{-1}, the cyclohexanone oxime N=O stretch at 1654 cm^{-1}, and the ε-caprolactam C=O stretch is at 1660 cm^{-1}) lie close in energy and are subject to variation through hydrogen bonding with the catalyst. The expectation that the C–H/N–H/O–H stretch region would be more informative is also not realized, and since the C–H stretch modes relate to methylene groups from all three molecules, their positions and relative intensities are similar. In addition, the hydrogen-bonded N–H and O–H vibrations are very susceptible to perturbation as the local environment changes from trimers in cyclohexanone oxime and dimers in ε-caprolactam, to individual molecules when hydrogen-bonded to the catalyst framework.

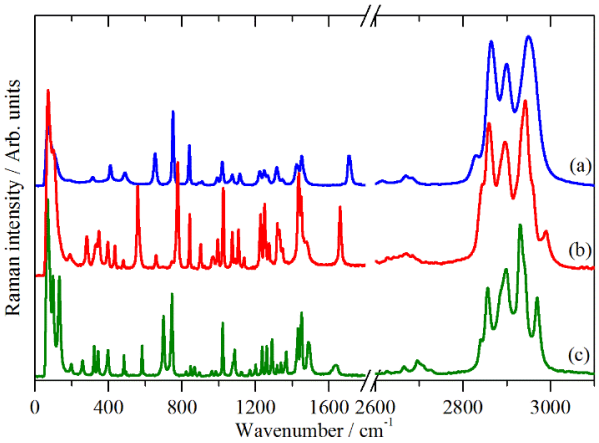

Figure 13. Comparison of room-temperature FT-Raman (**B**) spectra of: (a) cyclohexanone, (b) cyclohexanone oxime and (c) ε-caprolactam.

In the case of Raman spectroscopy, the situation is even worse, since the catalysts are invariably fluorescent, with either visible or near infrared excitation, preventing spectra from being obtained by conventional methods. Thus, INS spectroscopy is the only technique that can access the region below ~1600 cm^{-1}. As Figure 14 shows, the spectra of all three compounds are remarkably similar in the 1000 - 1600 cm^{-1} range, which is dominated by common methylene rock, wag, twist and scissors modes. The 100 - 1000 cm^{-1} encompasses the skeletal modes, including ring deformations and out-of-plane bending modes of the substituents. As the former involve the molecular framework, which is primarily C–C bonds, these modes are less susceptible to the influences of the external environment than those involving hydrogen bonding. Between 200 and 500 cm^{-1} cyclohexanone has three strong modes, cyclohexanone oxime has five and ε-caprolactam has four, thus providing a characteristic and unambiguous fingerprint of each species.

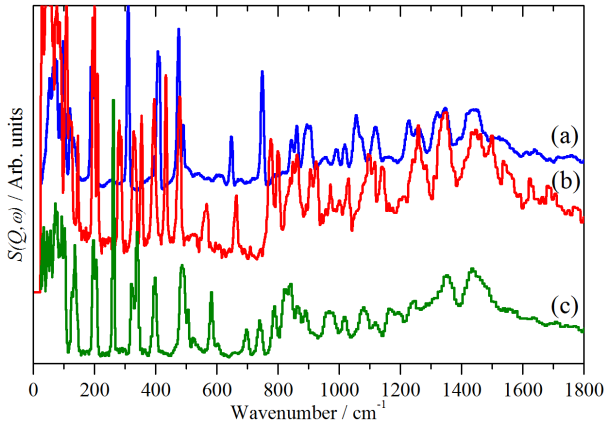

Figure 14. Comparison of TOSCA spectra at 10 K of: (a) cyclohexanone, (b) cyclohexanone oxime and (c) ε-caprolactam.

Conclusions

In optimizing heterogeneous acid catalysts for nylon-6 production, a molecular-level understanding of catalytic transformations will necessitate the use of *in situ* and *operando* spectroscopies. To aid such investigations, we have analyzed three key species associated with the Beckmann rearrangement step (cyclohexanone, cyclohexanone oxime and ε-caprolactam), using a range of complementary vibrational techniques. The spectroscopy of these molecules proved unexpectedly complex, particularly due to the polymorphism exhibited by cyclohexanone oxime. Nonetheless, a combination of infrared, Raman and INS spectroscopies, with assignments provided by periodic-DFT, has enabled complete characterization to be made. From this, we have identified the characteristic vibrational modes that can be used to track each species as they are transformed. Moreover, the work clearly highlights the advantage of INS spectroscopy for studies of adsorbed species, it being the only technique capable of accessing the characteristic modes that are relatively independent of the surrounding environment.

Experimental Section

Materials: Cyclohexanone (≥99 %, Sigma Aldrich), cyclohexanone oxime (97 %, Sigma Aldrich) and ε-caprolactam (99 %, Sigma Aldrich) were used as received. ε-Caprolactam-D10 (0.50 g, 99% D), $C_6D_{10}NOH$, was purchased from QMX Laboratories Ltd.. Cyclohexanone-D10 oxime was synthesized by reacting a 1:1 molar ratio of cyclohexanone-D10 (99% D, Sigma Aldrich) and hydroxylamine (50 wt. % in H_2O, Sigma Aldrich) in an ice bath under stirring. After 1 hour, the white solid was collected by vacuum filtration, washed with ice-cold, deionized water (200 mL), and then dried under vacuum. The synthesis and characterization of the product is described in more detail in the Supplementary Information (Figures S1-S3).

Vibrational Spectroscopy: FT-Raman spectra were recorded at room temperature with a Bruker MultiRam spectrometer using 1064 nm excitation, 4 cm^{-1} resolution, 500 mW laser power and 1024 scans. Variable temperature Raman spectra (10 – 300 K) were recorded using 785 nm excitation with a custom modified Renishaw InVia spectrometer, that has been previously described.[29] The infrared spectra were recorded using a Bruker Vertex70 FTIR spectrometer, 4 cm^{-1} resolution with a DLaTGS detector using 64 scans and at room temperature for the range 50 to 4000 cm^{-1} with a Bruker Diamond ATR and variable temperature (150 – 300 K) over the range 350 to 4000 cm^{-1} with a Specac Golden Gate ATR with the variable temperature option. INS spectroscopy was carried out on the high resolution broadband spectrometer TOSCA[30] and the direct geometry spectrometer MAPS[31] at the ISIS Pulsed Neutron and Muon Facility[32] (Chilton, UK). The sample, 0.5 to 2.0 g, was loaded into a thin-walled aluminium cell, which was inserted into the closed cycle refrigerator of the spectrometer and cooled to < 20 K. The two spectrometers are complementary;[31] for the present work the key features are that TOSCA provides good resolution spectra from 0 – 2000 cm^{-1}, while MAPS enables observation of the O–H and C–H stretch region.

Computational Methods: The plane wave pseudopotential based program CASTEP was used for the calculation of the vibrational transition energies and their intensities.[33] The generalized gradient approximation (GGA) Perdew-Burke-Ernzerhof (PBE) functional was used in conjunction with optimized norm-conserving pseudopotentials. The source of the starting structures, details of the plane-wave cut-off and the Monkhorst-Pack grids that were used are given in Table S1 of the Supporting Information. All calculations were converged to better than |0.0078| eV $Å^{-1}$. After geometry optimization, the vibrational spectra were calculated in the harmonic approximation using density-functional perturbation-theory.[34] This procedure generates the vibrational eigenvalues and eigenvectors, which allows visualization of the modes within Materials Studio[35] or by Jmol[36] and is also the information needed to calculate the INS spectrum using the program ACLIMAX.[37] Transition energies for isotopic species were calculated from the dynamical matrix that is stored in the CASTEP checkpoint file using the PHONONS utility.[38] We emphasize that none of the transition energies have been scaled.

Acknowledgements

UK Catalysis Hub is kindly thanked for resources and support provided via our membership of the UK Catalysis Hub Consortium and funded by EPSRC (EP/K014714/1). The STFC Rutherford Appleton Laboratory is thanked for access to neutron beam facilities. Computing resources (time on the SCARF compute cluster for the CASTEP calculations) was provided by STFC's e-Science facility. This research has been performed with the aid of

facilities at the Research Complex at Harwell including the FT-Raman spectrometer. AJOM would like to acknowledge the Ramsay Memorial trust for provision of a Ramsay Fellowship. SC thanks AdvanSix Inc. for their support in funding her PhD studentship.

Keywords: Neutron spectroscopy • Infrared spectroscopy • Raman spectroscopy • catalysis

[1] M. Misra, J. K. Pandey, A. Mohanty, *Biocomposites: Design and Mechanical Performance*, Elsevier Science, Cambridge, **2015**.

[2] Polyamide 6 (Pa6) - Global Trends, Estimates and Forecasts, 2012-2018. http://www.prnewswire.com/news-releases/polyamide-6-pa6---global-trends-estimates-and-forecasts-2012-2018-300092015.html**, 2015**.

[3] Nylon 6 & 66 Market Size Worth $41.13 Billion by 2025 | Cagr: 6.1%. Grand View Research, http://www.grandviewresearch.com/press-release/global-nylon-6-66-market, **2017**.

[4] J. Ritz, H. Fuchs, H. Kieczka, W. C. Mora, *Ullmann's Encyclopedia of Industrial Chemistry*, 6 ed., Wiley-VCH, Weinheim, **2002**.

[5] S. Chapman, M. Potter, R. Raja, *Molecules* **2017**, *22*, 2127.

[6] R. A. Sheldon, R. S. Downing, *Appl. Catal. A Gen.* **1999**, *189*, 163-183.

[7] I. Yoshitaka, I. Hiroshi, S. Yasumoto, K. Masaru, S. Hiroshi, *Bull. Chem. Soc. Jpn.* **2007**, *80*, 1280-1287.

[8] a) S. H. Newland, W. Sinkler, T. Mezza, S. R. Bare, M. Carravetta, I. M. Haies, A. Levy, S. Keenan, R. Raja, *ACS Catal.* **2015**, *5*, 6587-6593; b) M. E. Potter, S. Chapman, A. J. O'Malley, A. Levy, M. Carravetta, T. M. Mezza, S. F. Parker, R. Raja, *ChemCatChem* **2017**, *9*, 1897-1900; c) M. E. Potter, A. J. O'Malley, S. Chapman, J. Kezina, S. H. Newland, I. P. Silverwood, S. Mukhopadhyay, M. Carravetta, T. M. Mezza, S. F. Parker, C. R. A. Catlow, R. Raja, *ACS Catal.* **2017**, *7*, 2926-2934.

[9] a) H. Fuhrer, V. B. Kartha, P. J. Krueger, H. H. Mantsch, R. N. Jones, *Chem. Rev.* **1972**, *72*, 439-456; b) Y. Huang, D. F. R. Gilson, I. S. Butler, *J. Phys. Chem.* **1993**, *97*, 1998-2001; c) F. J. Devlin, P. J. Stephens, *J. Phys. Chem. A* **1999**, *103*, 527-538; d) P. D. Vaz, P. J. A. Ribeiro · Claro, *J. Raman Spectrosc.* **2003**, *34*, 863-867.

[10] a) S. Hiroshi, H. Ken-ichi, N. Yasuo, *Chem. Lett.* **1993**, *22*, 1987-1990; b) C. Flego, L. Dalloro, *Micropor. Mesopor. Mater.* **2003**, *60*, 263-271.

[11] a) D. H. Zaitsau, Y. U. Paulechka, G. J. Kabo, A. N. Kolpikau, V. N. Emel'yanenko, A. Heintz, S. P. Verevkin, *J. Chem. Eng. Data* **2006**, *51*, 130-135; b) D. H. Zaitsau, Y. U. Paulechka, G. J. Kabo, A. V. Blokhin, V. N. Emel'yanenko, S. P. Verevkin, A. Heintz, *J. Chem. Eng. Data* **2008**, *53*, 694-703.

[12] P. R. Olivato, D. S. Ribeiro, J. Zukerman-Schpector, G. Bombieri, *Acta Crystallogr. B* **2001**, *57*, 705-713.

[13] P. Mani, S. Suresh, C. Revathi, *Asian J. Chem.* **2010**, *22*, 2653.

[14] S. Ramalingam, M. Karabacak, S. Periandy, N. Puviarasan, D. Tanuja, *Spectrochim. Acta A Mol. Biomol. Spectrosc.* **2012**, *96*, 207-220.

[15] a) N. E. Triggs, J. J. Valentini, *J. Phys. Chem.* **1992**, *96*, 6922-6931; b) N. E. Triggs, R. T. Bonn, J. J. Valentini, *J. Phys. Chem.* **1993**, *97*, 5535-5540; c) Y. Wang, T. G. Spiro, *Biophys. Chem.* **2003**, *105*, 461-470; d) I. A. Garbuzova, B. V. Lokshin, *Russ. Chem. Bull.* **2004**, *53*, 1894-1902.

[16] R. Ibberson, *Acta Crystallogr. B* **2006**, *62*, 592-598.

[17] O. Yoshitake, K. Kunio, *Bull. Chem. Soc. Jpn.* **1968**, *41*, 1323-1325.

[18] J. Dillen, H. J. Geise, *J. Mol. Struct.* **1980**, *69*, 137-144.

[19] O. Yoshiharu, S. Akira, N. Isamu, *Bull. Chem. Soc. Jpn.* **1956**, *29*, 210-212.

[20] C. M. López, K. Rodríguez, B. Méndez, A. Montes, F. J. Machado, *Appl. Catal. A Gen.* **2000**, *197*, 131-139.

[21] N. Colthup, *Introduction to Infrared and Raman Spectroscopy*, Elsevier Science, **2012**.

[22] M. Lutz, A. L. Spek, R. Dabirian, C. A. van Walree, L. W. Jenneskens, *Acta Crystallogr. C Cryst. Struct. Commun.* **2004**, *60*, 127-129.

[23] G. J. Kearley, M. R. Johnson, *Vib. Spectrosc.* **2010**, *53*, 54-59.

[24] P. W. Albers, J. Glenneberg, K. Refson, S. F. Parker, *J. Chem. Phys.* **2014**, *140*, 164504.

[25] M. Krzystyniak, K. Druzbicki, F. Fernandez-Alonso, *Phys. Chem. Chem. Phys.* **2015**, *17*, 31287-31296.

[26] E. K. Gibson, J. Callison, J. M. Winfield, A. Sutherland, R. H. Carr, A. Eaglesham, S. F. Parker, D. Lennon, *Ind. Eng. Chem. Res.* **2018**, *57*, 7355-7362.

[27] G. J. Kabo, A. A. Kozyro, V. S. Krouk, V. M. Sevruk, I. A. Yursha, V. V. Simirsky, V. I. Gogolinsky, *J. Chem. Thermodyn.* **1992**, *24*, 1-13.

[28] F. K. Winkler, J. D. Dunitz, *Acta Crystallogr. B* **1975**, *31*, 268-269.

[29] M. A. Adams, S. F. Parker, F. Fernandez-Alonso, D. J. Cutler, C. Hodges, A. King, *Appl. Spectrosc.* **2009**, *63*, 727-732.

[30] S. F. Parker, F. Fernandez-Alonso, A. J. Ramirez-Cuesta, J. Tomkinson, S. Rudic, R. S. Pinna, G. Gorini, J. F. Castañon, *J. Phys. Conf. Ser.* **2014**, *554*, 012003.

[31] S. F. Parker, D. Lennon, P. W. Albers, *Appl. Spectrosc.* **2011**, *65*, 1325-1341.

[32] http://www.isis.stfc.ac.uk/index.html

[33] K. Refson, P. R. Tulip, S. J. Clark, *Phys. Rev. B* **2006**, *73*, 155114.

[34] M. Victor, P. Alexander, R. Keith, J. C. Stewart, G. Jacob, W. Bjoern, *J. Phys. Condens. Matt.* **2009**, *21*, 485404.

[35] Materials Studio, http://accelrys.com/products/materials-studio/

[36] Jmol: An Open-Source Java Viewer for Chemical Structures in 3D. http://www.jmol.org/.

[37] A. J. Ramirez-Cuesta, *Comput. Phys. Commun.* **2004**, *157*, 226-238.

[38] K. Refson, Phonons and Related Calculations in CASTEP, http://www.castep.org/.

Supplementary Information for:

Comprehensive vibrational spectroscopic characterization of nylon-6 precursors for precise tracking of the Beckmann rearrangement

Stephanie Chapman, Alexander J. O'Malley, Stewart F. Parker, and Robert Raja

Contents **Page**

Figures S1 – S3. Preparation and characterization of cyclohexanone-D10 oxime. 2

Table S1. Computational details for the compounds studied. 5

Figure S4. Calculated dispersion curves of cyclohexanone in Phase III. 5

Scheme S1. Numbering system for the carbon skeletons of cyclohexanone, cyclohexanone oxime and ε-caprolactam used in Tables S2-S4. 6

Table S2. Transition energies and assignments for cyclohexanone. 6

Figure S5. DSC data for the compounds. 9

Figure S6. Infrared spectra of cyclohexanone oxime. 10

Figure S7. Raman spectra of cyclohexanone-D10 oxime. 10

Figure S8. Observed and calculated INS spectra of cyclohexanone oxime and cyclohexanone-D10 oxime in Phase III. 11

Figure S9. Observed and calculated infrared spectra of cyclohexanone oxime. 12

Table S3: Transition energies (cm^{-1}) and assignments for cyclohexanone oxime and cyclohexanone-D10 oxime in Phase III. 13

Table S4: Transition energies (cm^{-1}) and assignments for ε-caprolactam and ε-caprolactam-D10. 19

References 24

Preparation and characterization of cyclohexanone oxime-D10

The deuterated D_{10} analogue of cyclohexanone oxime was synthesized from hydroxylamine and cyclohexanone-D_{10}. Gas chromatography (GC) indicated phase-pure oxime at a retention time of 6.7 min (as for hydrogenous oxime) in ethanol (**Figure S1**). In order to confirm that the compound prepared from cyclohexanone and hydroxylamine was indeed cyclohexanone oxime, the material was tested in the liquid-phase Beckmann rearrangement using a hierarchical AlPO-5 catalyst (Figure S2). GC analysis indicated that synthesized D_{10}-oxime reacted in a manner analogous to commercial cyclohexanone oxime (Figure S3).

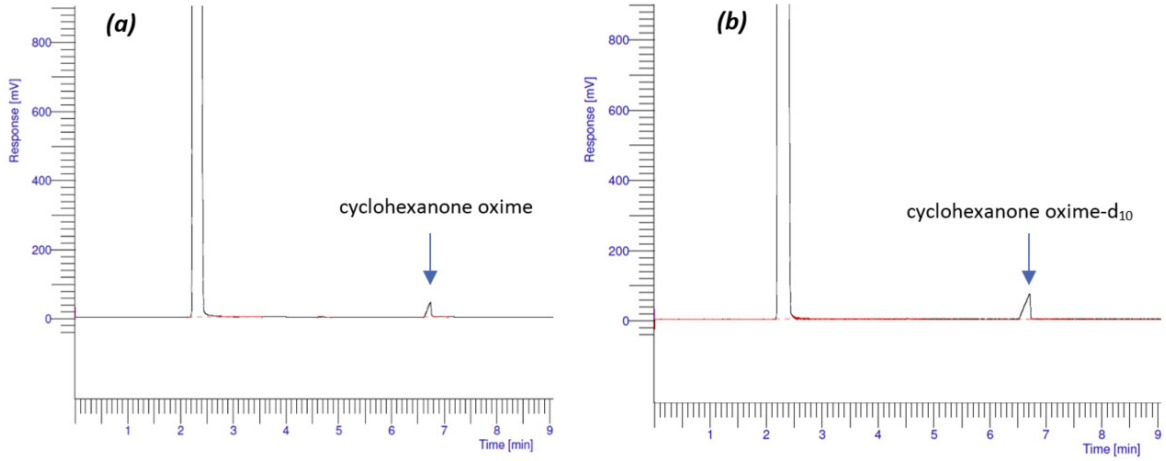

Figure S1. GC trace for hydrogenous cyclohexanone oxime (a) and deuterated cyclohexanone oxime-D_{10} (b) dissolved in ethanol.

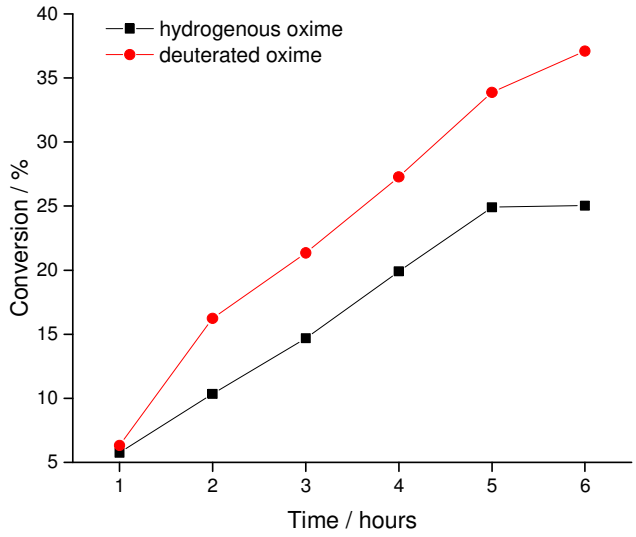

Figure S2. Percent conversion of hydrogenous (black line) and deuterated (red line) cyclohexanone oxime in the liquid-phase Beckmann rearrangement (130 °C, 6 hours, anhydrous benzonitrile solvent).

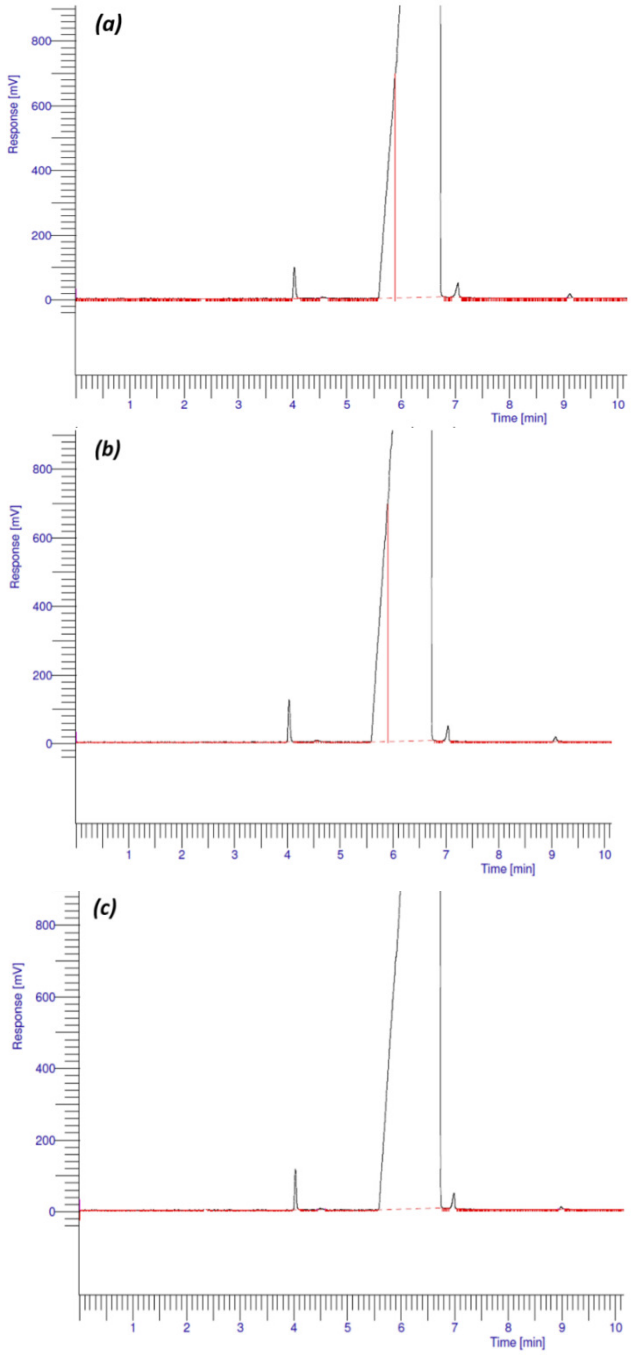

Figure S3. GC trace after 6 hours of liquid-phase Beckmann reaction with hierarchical AlPO-5 catalyst using commercial hydrogenous cyclohexanone oxime (a), synthesised hydrogenous cyclohexanone oxime (b) and D_{10} cyclohexanone oxime (c).

Table S1 Computational details for the compounds studied.

Metal	Source of initial structure (ref and CSD refcode [1])	Plane wave cutoff / eV	Monkhorst-Pack grid	Number of k-points
Cyclohexanone	[2] ZZZWGK02	1000	6×8×10	120
Cyclohexanone oxime	[3] ZZZVPO03	830	2×2×6	6
Cyclohexanone oxime trimers	Adapted from ZZZVPO03	880	2×2×6	12
ε Caprolactam	[4] CAPLAC	830	4×4×6	30

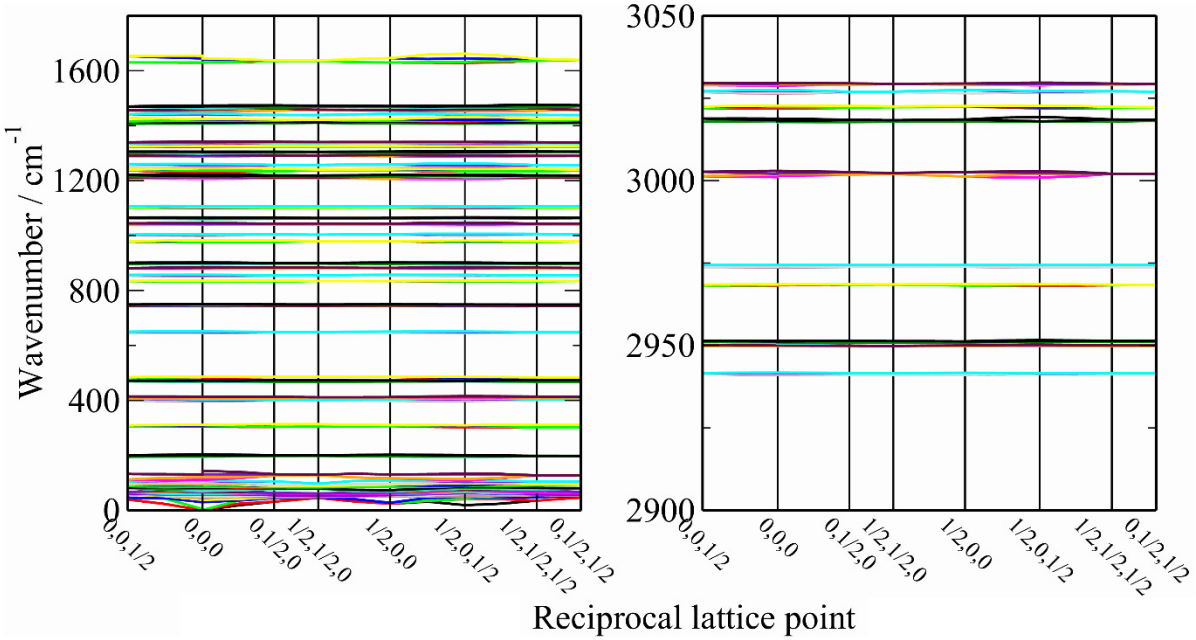

Figure S4. Calculated dispersion curves of cyclohexanone in Phase III.

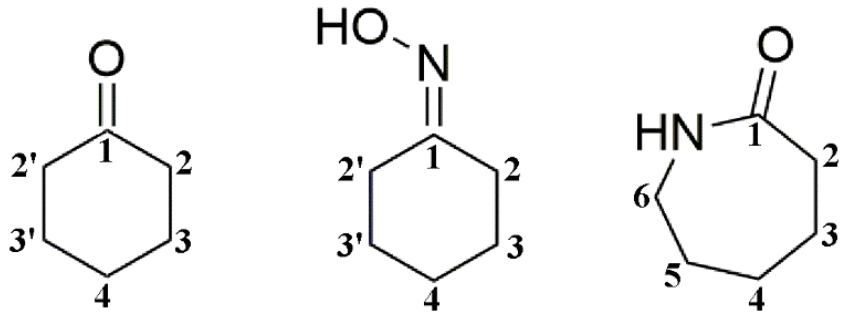

Scheme S1: Numbering system for the carbon skeletons of: cyclohexanone (left) in Table S2, cyclohexanone oxime (center) in Table S3 and ε-caprolactam (right) in Table S4.

Table S2: Transition energies (cm-1) and assignments for cyclohexanone in the 0–1800 cm-1 region in Phase III.

Cyclohexanone			Assignment
Raman[a]	INS	CASTEP	
56 m	53 m	0,0,0,29	Acoustic and optic translation
	64 m	38,50,61,68	Libration ⊥ to ring
64 w, 70 m	74 s	64,64,87,93,	Optic translation
82 m	87 m	70,82,95,97	Libration // to C=O
92 s	97 s	58,79,85,101	Libration ⊥ to C=O
107 m, 119 m	120 m	45,66,110,120	Optic translation
144 w	131 w	107,108,130,131	C=O out-of-plane bend
205 w	188 s, 203 s	195,196,201,203	C2–C3 + C2′–C3′ out-of-phase torsion
307 w	310 vs	305,308,309,311	C3–C4 + C3′–C4′ in-phase torsion
404 w		398,400,401,404	C2–C3 + C2′–C3′ in-phase torsion
412 w, 420 w	407 s, 412 m	410,410,412,413	C3–C4 + C3′–C4′ out-of-phase torsion
473 w	475 s	467,469,472,473	C1–C2 + C1–C2′ in-phase torsion
492 m	490 m	484,485,486,487	C=O in-plane bend
647 s	647 m	646,647,649,651	C2–C1–C2′ bend
		742,743,744,745	C2 + C2′ + C3′ out-of-phase rock
751 vs	748 s	748,749,750,750	C2 + C2′ + C3 out-of-phase rock
845 s	843 m	832,833,837,837	C3–C4 + C3′–C4 in-phase stretch
	861 m	851,856,856,858	C2 + C2′ in-phase rock
894 vw	896 m	879,880,882,884	C3 + C3′ out-of-phase rock
906 w	905 m	895,900,900,902	C4 wag
995 w	991 w	976,977,983,983	C2–C3 + C2′–C3′ in-phase stretch

1016 w, 1021 s	1018 w	1000,1003,1003,1005	C1–C2 + C1–C2′ in-phase stretch
		1040,1041,1041,1045	C1 + C1′ + C4 out-of-phase methylene twist
1052 vw	1056 m	1060,1063,1065,1066	C3–C4 + C3′–C4 out-of-phase stretch
1072 s	1073 sh	1101,1101,1102,1104	C4 rock
1113 w, 1122 w	1120 m, br	1105,1106,1107,1108	C2 + C2′ out-of-phase methylene twist
		1207,1208,1211,1214	C2 + C2′ in-phase methylene twist
1220 sh, 1226 m		1215,1215,1216,1223	C1–C2 + C1–C2′ out-of-phase stretch
1234 w	1226 m	1231,1237,1244,1245	C3 + C3′in-phase methylene twist and C2 + C2′ in-phase methylene wag
1249 w, 1256 m	1260 m, br	1249,1252,1256,1261	C1 + C1′ + C4 in-phase methylene twist
1265 m, 1269 sh		1288,1289,1291,1294	C2 + C2′ out-of-phase methylene wag and C3 + C3′ out-of-phase methylene twist
		1299,1303,1304,1306	C2 + C2′ in-phase methylene wag and C3 + C3′in-phase methylene twist
1315 w	1319 w	1323,1325,1325,1326	C4 methylene wag
1325 w		1334,1337,1337,1338	C3 + C3′ out-of-phase methylene wag
1352 m	1347 m	1338,1339,1340,1343	C3 + C3′in-phase methylene wag
1411 m,1418 m		1407,1408,1412,1417	C2 + C2′ out-of-phase methylene scissors
1432 m	1439 m vbr	1418,1419,1423,1424	C2 + C2′in-phase methylene scissors
1445 m		1440,1441,1441,1445	C4 methylene scissors
1462 w		1453,1454,1458,1459	C3 + C3′ out-of-phase methylene scissors
		1463,1469,1470,1474	C3 + C3′in-phase methylene scissors
1697 m, 1704 w		1629,1630,1642,1645	C=O stretch

[a]s = strong, m = medium, w = weak, v = very, sh = shoulder, br = broad, v = very.

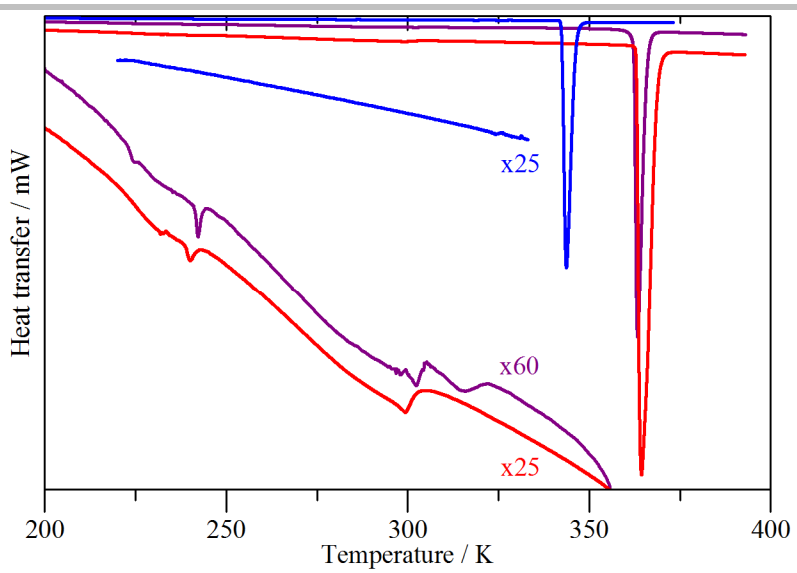

Figure S5. DSC data for cyclohexanone oxime (red), cyclohexanone-D10 oxime (purple) and ε-caprolactam (blue).

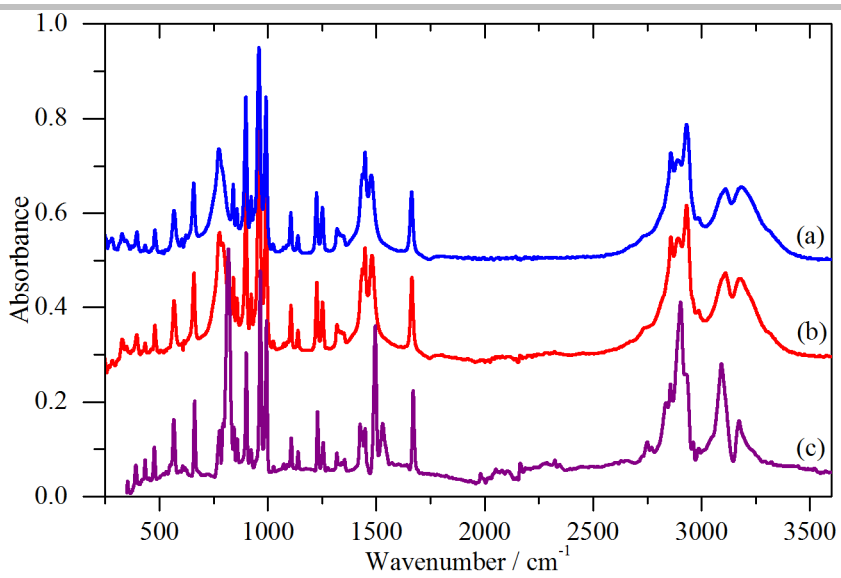

Figure S6. Infrared spectra of cyclohexanone oxime in (a) Phase I, 323 K, (b) Phase II, 286 K and (c) Phase III, 150 K.

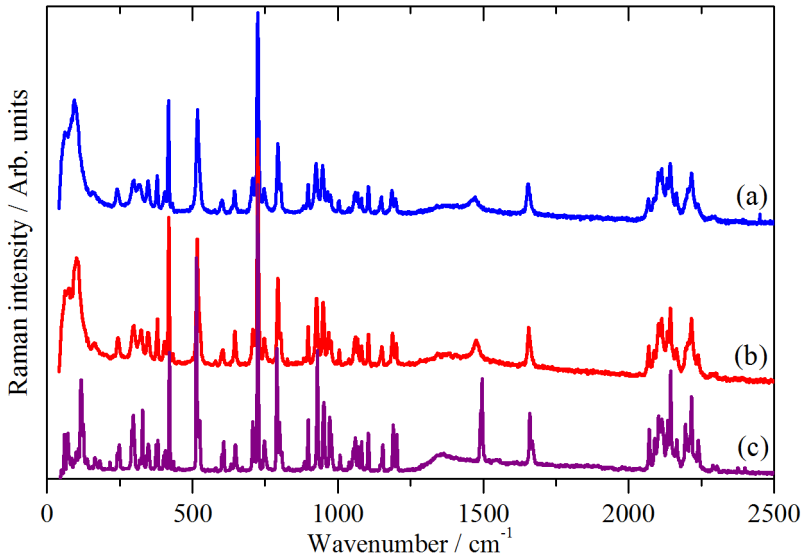

Figure S7. Raman spectra of cyclohexanone-D10 oxime in (a) Phase I, 330 K, (b) Phase II, 270 K and (c) Phase III, 10 K.

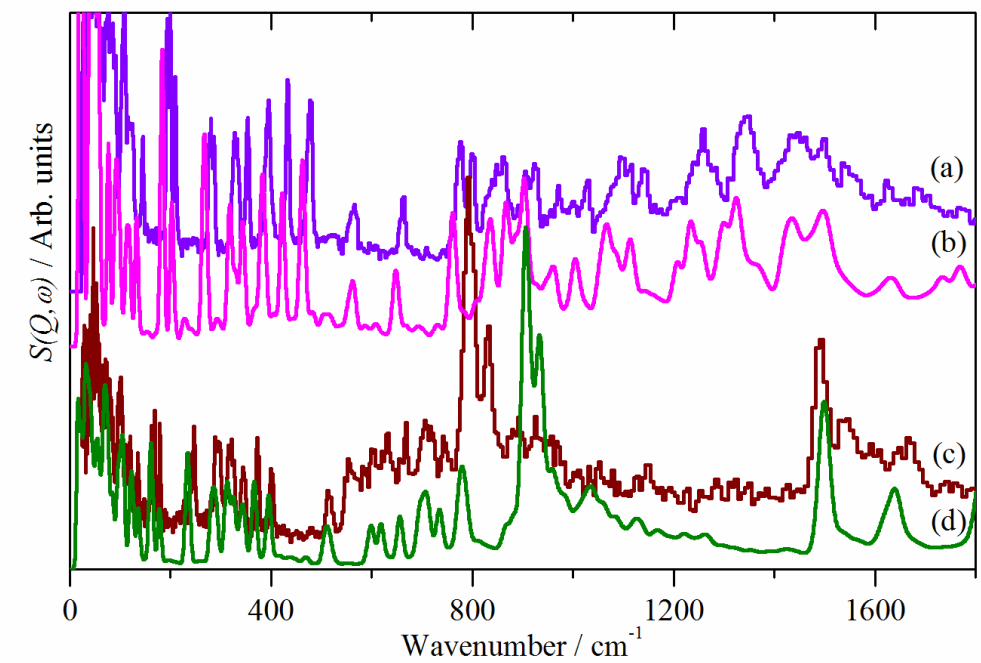

Figure S8. INS spectra in Phase III at 10 K of (a) cyclohexanone oxime, (b) cyclohexanone oxime as calculated using CASTEP of the CCI trimer shown in Figure 5 of the main text, (c) cyclohexanone-D10 oxime and (d) as (b) for the D10 species. Note that (c) is ×11 ordinate expanded relative to (a), reflecting the difference in cross section between H and D.

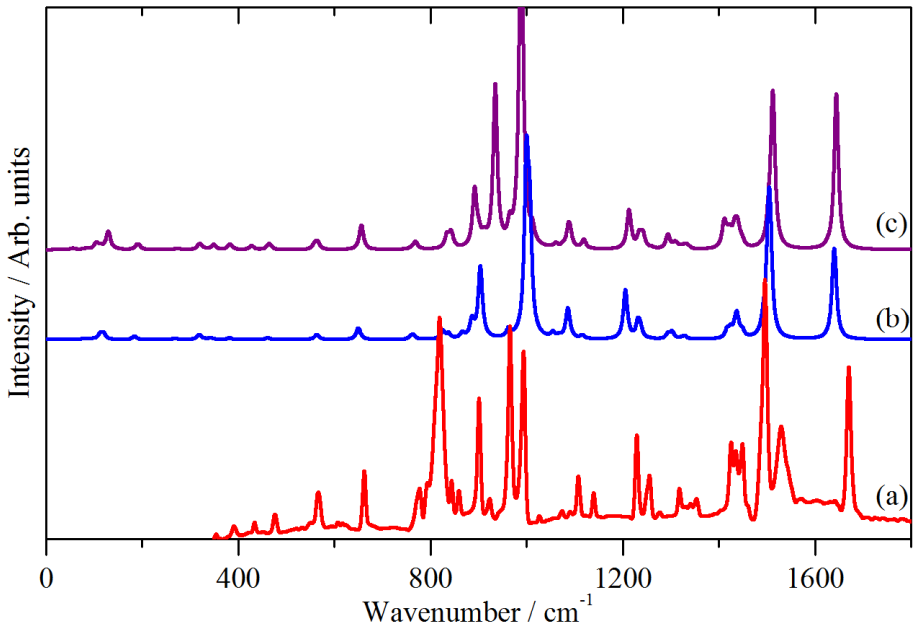

Figure S9. Infrared spectra of cyclohexanone oxime in Phase III at 10 K: (a) experimental, (b) calculated for the CCI trimer shown in Figure 5 of the main text and (c) calculated for the complete unit cell of 342 atoms.

Table S3: Transition energies (cm^{-1}) and assignments for cyclohexanone oxime and cyclohexanone-D10 oxime in Phase III.

Cyclohexanone oxime					Cyclohexanone-D10 oxime					Assignment
Infrared[a,b]	Raman	INS	CASTEP[c]		Infrared[b]	Raman	INS	CASTEP		
			Average[c]	Δ[d]				Average	Δ	
		29 s	24	41				22	38	Translation
50 vw		41 s	40	15				38	14	Translation
53 vw, 60 w, 67 w	65 m	50 s, 56 m, 59 sh, 65 w	60	21	58 w, 65 w	50 vw, 60 w	50 s,br	55	19	Translation
76 w	78 m, 85 w		78	11		71 w, 78 w	74 m,br	71	9	Libration // to N=O
88 sh		90 w	94	21	87 sh	85 w, 93 w		87	22	Libration ⊥ to N=O
107 m,br	108 w, 119 s	108 s, 116 m	111	8	100 m,br	100 w, 107 w, 116 s, 125 m	96 m, 101 m, 104 m, 110 w, 120 w	105	7	C=N torsion
144 w	125 sh, 130 w, 148 w	125 m, 145 m	136	24		138 w	135 m	128	19	Libration ⊥ to ring
192 w	195 w, 202 vw, 210 vw, 215 vw	194 s, 200 s, 210s	197	23	156 sh, 163 w	165 w, 170 w, 181 w	163 w, 169 m, 180 m	168	21	C2–C3 + C2′–C3′ out-of-phase torsion
282 w	281 m, 289 w	279 s, 287 m	274	11	242 w	241 w, 249 w	240 w, 247 m	235	6	C3–C4 + C3′–C4′ in-phase torsion

327 w	329 m, 334 w	327 s, 332 m	323	14	295 w	292 w, 296 w	290 w, 297 m	287	13	C2–C3 + C2′–C3′ in-phase torsion
354 w	352 m, 356 m	354 s	349	8	319 w	319 vw, 328 w	316 m, 325 m	318	18	N–C1–C2 out-of-plane bend
391w	393 w	395 s,br	385	9	345 w	343 sh, 349 w	343 m,br	343	11	C1–C2 + C1–C2′ in-phase torsion
434 w	434 m	433 s	428	2	374 w	375 w, 382 w	373 m	367	5	C3–C4 + C3′–C4′ out-of-phase torsion
477 w	480 w	479 s,br	465	6	402 vw	401 w, 407 w	401 m	396	5	C1–C2 + C1–C2′ in-phase torsion
566 w	557 s, 567 w	564 m	558	17	519 m, 524 sh	514 s, 519 w, 525 w	513w,br	512	13	N–C1–C2 in-plane bend
662 w	663 w	662 m	654	7	579 w	579 vw	585 w	598	9	C2–C1–C2′ bend
776 w	772 s.	777 s	760	4	606 m	602 w, 608 w	602 w	619	2	C2 + C2′ out-of-phase rock
	782 s		770	5	668 w	671 vw	669 w	657	3	C2 + C2′ in-phase rock
819 s,br	800 w	800 m	921	29	786 m, 814 s,br	799 m, 791 w	790 s, 833 s	774	5	NO–H out-of-plane bend
844 w	846 m	839 w, 848 m	835	2	705 w	707 w	706 w,br	696	2	C3–C4 + C3′–C4 in-phase stretch
860 w	862 vw	862 m	844	4	713 w	715 w	719 w,br	706	4	C4 rock
901 s	906 m	907 m	893	4	724 sh	725 s		714	3	C2–C3 + C2′–C3′ out-of-phase stretch
922 w	922 vw	926 m	902	8	745 m	748 w	746 w	735	3	C3 + C3′ out-of-phase rock
965 vs	972 w, 977 w	970 w	967	6				780	4	C1–C2 + C1–C2′ in-phase stretch
			996	17	958 vs			976	13	N–O stretch
994 vs	999 m	1001 w	1011	5				788	4	C2 + C2′ in-phase wag

1026 w	1027 s	1027 w	1060	5	881 w	886 w		868	7	C3–C4 + C3′–C4 out-of-phase stretch
1072 w	1075 m	1075 w,br	1077	2				883	3	C2 + C2′ out-of-phase methylene twist
1092 w	1092 w	1097 m	1089	4	897 w	897 w		908	12	C2 + C2′ in-phase methylene twist
1108 m	1109 m	1114 m	1119	4	926 w	927 m		922	18	C3 + C3′ out-of-phase methylene twist
1139 w	1139 w	1141 m,br	1216	8	943 s	951 w		935	5	C2 + C2′ in-phase methylene twist
1228 m	1229 m	1231 m,br	1234	8	958 vs	971 w, 977 sh		959	7	C2 + C2′ in-phase methylene wag and C3 + C3′in-phase methylene twist
1254 m	1252 m, 1260 w	1260 m	1244	7	1005 vw	1007 vw		988	7	C4 methylene twist
1276 w	1276 w	1282 w	1259	4	1036 w	1040 vw		1023	3	C2 + C2′ out-of-phase methylene twist
1318 w	1318 w, 1322 w		1296	7	1058 w	1055 w, 1058 w		1036	4	C2 methylene wag
	1331 w		1311	9				1042	5	C2′ methylene wag
			1322	4				1053	3	C3 + C3′ out-of-phase methylene wag
1340 vw	1344 w		1330	2	1087 w	1082 w		1065	6	C4 methylene wag
1353 w	1350 w, 1357 w	1345 m,vbr	1336	3	1100 w	1104 w		1085	4	C3 + C3′in-phase methylene wag
			1412	7	1115 w	1104 w		1123	3	C2 + C2′ out-of-phase methylene scissors

1425 m	1427 w, 1432 w		1420	7	1147 w	1145 w, 1154 w		1135	5	C2 + C2′in-phase methylene scissors
1435 m	1437 sh		1434	5	1186 m	1192 w		1164	3	C3 + C3′ out-of-phase methylene scissors
1449 m	1449 w, 1451 w		1440	6	1201 w	1202 w		1178	2	C4 methylene scissors
1461 vw	1461 w		1450	8	1285 m			1265	6	C3 + C3′in-phase methylene scissors
1496 vs, 1529 s	1496 w, 1502 sh		1510	11	1481 s	1496 m	1491 s	1499	9	NO–H in-plane bend
1670 s	1665 w, 1672 sh		1638	21	1665 s	1660 m, 1668 w	1669 w	1634	24	C=N stretch
2904 s,br			2765[e]	1	2892 s			2765	1	O–H stretch (A)
3102 s,br			2852[e]	14	3084 s			2852	14	O–H stretch (E)
3179 s,br			2875[e]	27	3166 s, br			2876	29	O–H stretch (E)
2835	2839		2928	13				2135	8	C2′ symmetric methylene stretch
2855	2860, 2868		2940	3				2142	3	C2 symmetric methylene stretch
			2946	2				2145	2	C3 symmetric methylene stretch
	2885		2948	3				2147	1	C4 symmetric methylene stretch
	2899		2958	3				2153	3	C3′ symmetric methylene stretch

2928	2927		2986	5				2212	4	C3 asymmetric methylene stretch
	2942		2997	2				2221	1	C4 asymmetric methylene stretch
2961	2962		3006	2				2228	1	C3′ asymmetric methylene stretch
			3021	2				2235	1	C2 asymmetric methylene stretch
2985	2990		3037	4				2245	4	C2′ asymmetric methylene stretch

[a]s = strong, m = medium, w = weak, v = very, sh = shoulder, br = broad, v = very

[b]Infrared data for 0 – 400 cm^{-1} is for Phase I at 300 K.

[c]Average of the 18 factor group components.

[d]Difference between highest and lowest factor group components

[e]Average of the first, second and third group of six of the 18 factor group components. See text for details.

Table S4: Transition energies (cm^{-1}) and assignments for ε-caprolactam and ε-caprolactam-D10.

ε-Caprolactam					ε-Caprolactam-D10					Assignment
Infrared[a]	Raman	INS	CASTEP		Infrared	Raman	INS	CASTEP		
			Ave[b]	Δ[c]				Ave	Δ	
		32 w						25		Translation
		44 w	40	23			43 w	38	15	Libration
		55 w	60	11			53 w	55	10	Libration
67 vw	69s	74 s,br	72	8	61 w	68 vs	71 w, br	67	9	Translation
88 vw		93 m	83	14	83 w		87 w	78	11	Translation
	99 s	102 m	102	2	93 vw	93 s	95 w	96	1	Libration (2 components)
121 vw		126 m	128	14	110 vw			105	25	C=O out-of-plane bend
130 vw	133 s	136 s	146	2	126 w	127 vs		140	1	Libration (2 components)
195 w	198 w	196 s, 205 m	189	8	167 w	172 w	170 w, 179 w	164	7	C2–C3 + C4–C5 in-phase torsion
259 w	260 w	262 vs	250	2	218 w	218 w	221 m	211	3	C2–C3 + C4–C5 out-of-phase torsion
324 w	322 m	322 m	317	4	278 w	284 w	281 m	269	4	C1–C2–C3 + C4–C5–C6 in-phase bend
339 vw	344 m	339 s	330	3	297 m	299 w	298 m	292	2	C3–C4–C5 bend
398 w	398 m	398 s	387	6	358 m	357 w	358 m	347	4	C4–C5 + C5–C6 in-phase torsion
489 w	485 m	487 s	471	10	390 m	389 w	389 m	377	6	C3–C4 + C6–N in-phase torsion
506 m		506 w	490	20	452s	434 w	434 w, 455 w	438	24	C=O in-plane bend
583 m	584 m	583 s	571	3	526 s	529 w	530 w	517	1	C1–N–C6 bend

692 w	699 s	696 m	684	7	616 w	622 w	622 w	606	5	C3 rock
745 vw	746 s	740 m	729	5	652 m	656 s	655 w	642	4	C6 rock
		789 m	846	7			793 s	848	0	N–H out-of-plane bend (2 components)
802 m, br		822 m	876	3	801 s, br		833 s	885	4	N–H out-of-plane bend (2 components)
821 w	822 vw		807	3	672 m	676 s	675 w	661	4	C5 rock
840 sh	848 w	841 s	825	4	708 m	711 w	712 w	697	3	C4 rock
866 w	869 w	865 w	852	4	727 w	731 w	731 w	716	5	C2–C3 + C5–C6 out-of-phase stretch
892 w		888 w	880	4	751 m	752 w	753 w	740	1	C1–C2–C3 bend
962 w	963vw	958 m	945	3	766 m	768 w	770 w	754	1	
981 w	985 vw	974 m	966	4				802	3	C2 rock
1020 vw	1022 s	1019 w	1008	2	819 m	817 m		824	6	C4 methylene twist
1089 m	1089 m	1082 m	1062	5	840 w, 851 m	840 w, 854 w		835	3	C2–C3 + C5–C6 in-phase stretch
		1092 sh	1072	2	894 m	895 m	899 w	875	13	C4–C5 stretch
1125 m	1123 vw	1119 vw	1104	5	914 m	915 m	917 w	896	1	C3–C4 stretch
1166 vw	1171 vw	1162 w	1153	1				926	7	N–C6 stretch
1197 m	1201 w	1196 w	1180	1	948 s	949 m	946 w	932	5	Methylene twist: C2 + C3 + C4 out-of-phase with C5
1239 w	1236 m	1240 w	1223	9	970 s	969 m		956	5	Methylene twist: C2 + C4 out-of-phase with C3 + C5
1256 w	1260 m		1243	5	994 m	996 m		979	3	Methylene twist: C2 + C6 out-of-phase with C4

1290 w	1290 m		1277	2	1011 m	1014 w		995	3	Methylene twist: C3 out-of-phase with C5
1316 w	1317 w		1301	3	1053 w	1052 w		1035	6	Methylene twist: C4 out-of-phase with C6
1332 w	1338 w		1318	5	1117 w	1117 sh		1047	4	C2 methylene wag
1351 sh		1352 m	1335	3				1054	6	C3 methylene wag
1364 m	1366 m		1342	3	1133 m	1137 w		1061	5	C4 methylene wag
			1347	3				1080	5	C5 methylene wag
1417 m			1404	9	1408 vs	1426 m		1398	16	N–C6 stretch
1437 m	1433 s	1436 m,br	1420	4				1097	2	Methylene scissors: C2 out-of-phase with C6
1447 sh			1426	5				1112	4	C5 methylene scissors
	1452 s		1435	9	1174 s	1176 w		1153	2	C4 methylene scissors
1467 w			1444	3	1204 s	1206 w		1180	1	Methylene scissors: C2 out-of-phase with C4
			1458	12	1224 s	1226 w		1199	1	C3 methylene scissors
1487 w	1491 m		1480	9	1470 m	1484 w	1489 m	1467	10	N–H in-plane bend + C=O stretch
1656 vs	1638 w		1617	26	1644 vs, br	1631 w		1609	26	C=O stretch + N–H in-plane bend

					2895 w					Combination: C1–N stretch + N–H in-plane bend
3067 m,br					2932 m					Overtone: 2 × N–H in-plane bend
3199 m					3055 s	3054 vw	3049 m			Combination: C=O stretch + N–H in-plane bend
3294 w					3197 s	3184 vw	3180 m			Out-of-phase N–H stretch
					3280 w		3317 w			Overtone: 2 × C=O stretch

[a]s = strong, m = medium, w = weak, v = very, sh = shoulder, br = broad, v = very

[b]Average of the four factor group components.

[c]Difference between highest and lowest factor group components.

References

1. Groom, C. R.; Bruno, I. J.; Lightfoot M. P.; Ward, S. C. The Cambridge Structural Database. *Acta Cryst.* 2016 *B72* 171-179.

2. Ibberson, R., The Low-Temperature Phase III Structure and Phase Transition Behaviour of Cyclohexanone. *Acta Crystallogr. B* 2006, *62*, 592-598.

3. Lutz, M.; Spek, A. L.; Dabirian, R.; van Walree, C. A.; Jenneskens, L. W., Twinning by Merohedry in Cyclohexanone Oxime: A Revised Structure. *Acta Crystallogr. C: Cryst. Struct. Commun.* 2004, *60*, 127-129.

4. Winkler, F. K.; Dunitz, J. D., Medium-Ring Compounds. XIX. Caprolactam: Structure Refinement. *Acta Crystallogr. B* 1975, *31*, 268-269.